Elementary and advanced modelling of the splitting strength of timber connections

J.C.M. Schoenmakers
Eindhoven University of Technology, the Netherlands

The load-bearing capacity of a timber member loaded perpendicular-to-grain by a connection is governed by either the embedment strength, the bending yield strength of the steel fasteners, or the splitting strength of the timber. Only coarse models for predicting the splitting strength are implemented in structural design codes, if any. It is of great importance for engineers to avoid splitting failure because it is often a brittle failure mode. This paper presents an overview of analytical, numerical and experimental research on the splitting strength of timber connections loaded perpendicular-to-grain by mechanical connections, conducted at Eindhoven University of Technology.

Based on the theory of fracture mechanics an analytical expression for predicting the splitting strength is derived. This analytical expression is applied to members loaded by a single connection composed of dowel-type fasteners such as nails, dowels and bolts. The expression is calibrated with experimental results, after which its prediction ability is verified using another set of experimental data. For this purpose, performed experiments as well as results presented in literature are used (new experiments should be considered complementary in most cases). To confirm the physical behaviour predicted by the analytical expression, a numerical study is performed based on linear and non-linear fracture mechanical finite element models. From this it follows that the energy associated with fracture of connections perpendicular-to-grain is close to the mode *I* fracture energy. Amongst others, the number of fasteners and the loaded edge distance of the furthest row of fasteners are significant parameters.

Key words: Timber, fracture mechanics, connections, equilibrium state, splitting strength

1 Introduction

The problem involved with mechanical connection with dowel-type fasteners (*e.g.* nails, dowels) is the development of stress concentrations at the interface between fasteners and timber. High local peak stresses cause high stress gradients in the vicinity of the fastener, to which timber is vulnerable due to its low strength properties, in particular perpendicular-to-grain. Therefore, tension forces perpendicular to the grain should be avoided. However, this is not always possible as show in Figure 1.

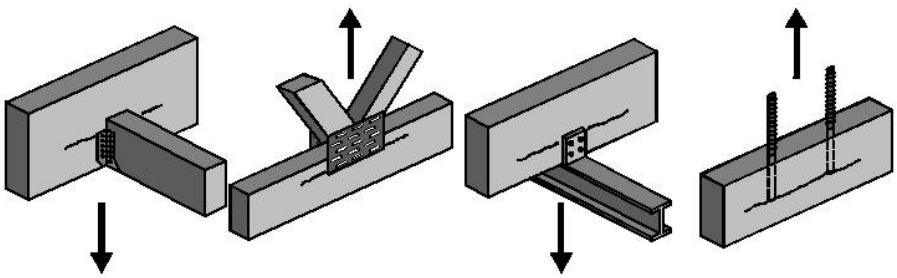

Figure 1. Timber elements exposed to tension forces perpendicular-to-grain by mechanical connections (Re-sketched after Ehlbeck and Görlacher (1995))

The connections of Figure 1 load the horizontal member in tension perpendicular-to-grain and shear, what may result in crack initiation and propagation parallel-to-grain direction. This may limit the load-bearing capacity considerably. Splitting failure of timber can be characterized as a brittle failure mechanism, which results in sudden failure of the structural element without warning by means of excessive deformation prior to structural collapse. Therefore, crack initiation and propagation are key factors in the behaviour of such connections and important for building practice regarding safety. In addition to splitting failure (fracture), the connection itself can be governing the load-bearing capacity what typically is a different failure mechanism. Hence, the lowest of either the connection capacity and the splitting capacity determines the load-bearing capacity.

The objective of this research is to develop improved design rules to account for the splitting failure mechanism (fracture) induced by mechanical connections perpendicular-to- grain. Increased predictability of the load-bearing capacity in various applications results in more transparent safety margins and in more cost-effective structures as conservatism in design can be minimized. This can improve the overall safety of connections applied in timber structures. Also reduction of timber element dimensions

may be possible in some cases, for instance by a reduction of the number of fasteners leading to smaller connections and consequently, less timber is needed to satisfy the minimum requirements for edge and end distances and spacing.

Comprehensive experimental investigations (in total up to 900 experiments) regarding the splitting capacity have been reported in literature (*e.g.* Möhler and Lautenschläger (1978), Ehlbeck and Görlacher (1983) and Ballerini and Giovanella (2003), amongst others). Also models for the load-bearing capacity in case of splitting failure have been reported (*e.g.* Van der Put (1992b) and Van der Put and Leijten (2000), Jensen (2003), Jensen *et al.* (2003)). Some are based on theoretical considerations (Fracture Mechanics - FM). Most experimental programs lack to recognize the different failure mechanisms. Hence, models to predict the splitting capacity often do not correspond to the experimental observations since other failure mechanisms than splitting have been taken into consideration. This is clarified in chapter 2.

Analysis of the embedment strength and the bending yield strength of steel fasteners are not included in this paper. These subjects are studied in Schoenmakers (2010).

2 Differences between fracture and other failure mechanisms

For clarification, a case study is presented in this section. The case under consideration is shown in Figure 2 where the dowel-type fasteners are loaded in double shear. The beam cross sectional area equals $t\,h$ = 45 × 222 mm² and the span l = 1600 mm. The relative height α is defined as the ratio of the loaded edge distance from the furthest row h_e of fasteners and the beam depth h, therefore, $\alpha = \frac{h_e}{h}$.

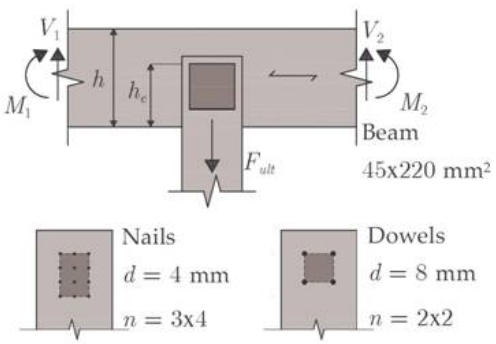

Figure 2. Situation discussed including two possible fastener configurations

The governing failure mechanism appears to depend on only three parameters, namely the number of fasteners, fastener diameter and relative height. Figure 3 shows the ultimate failure load as function of the number of fasteners, based on the analytical expressions corresponding to each failure mechanism (Schoenmakers (2010)). For comparison, similar situations are included with different fastener diameter d. A small number of fasteners (*e.g.* $n < 4$) results usually in relatively high embedment stresses underneath the dowel type fasteners. High embedment stresses usually result in a ductile failure mechanism since the embedment strength is reached prior to reaching the splitting strength. If the number of fasteners is increased (*e.g.* $n > 15$) the embedment stresses are usually rather low and hence, the splitting strength of the member is reached prior to reaching the embedment strength. Since the embedment strength increases with deceasing fastener diameter, the diameter is of high importance as well. Aside from connection failure, conventional failure mechanisms such as bending of the timber member may be governing as well. Yet, the fastener diameter (in relation to the timber width) also determined whether crushing of the timber (EYM I, fastener remains straight) or yielding of the fastener (EYM IV, plastic hinges in the fastener) occurs.

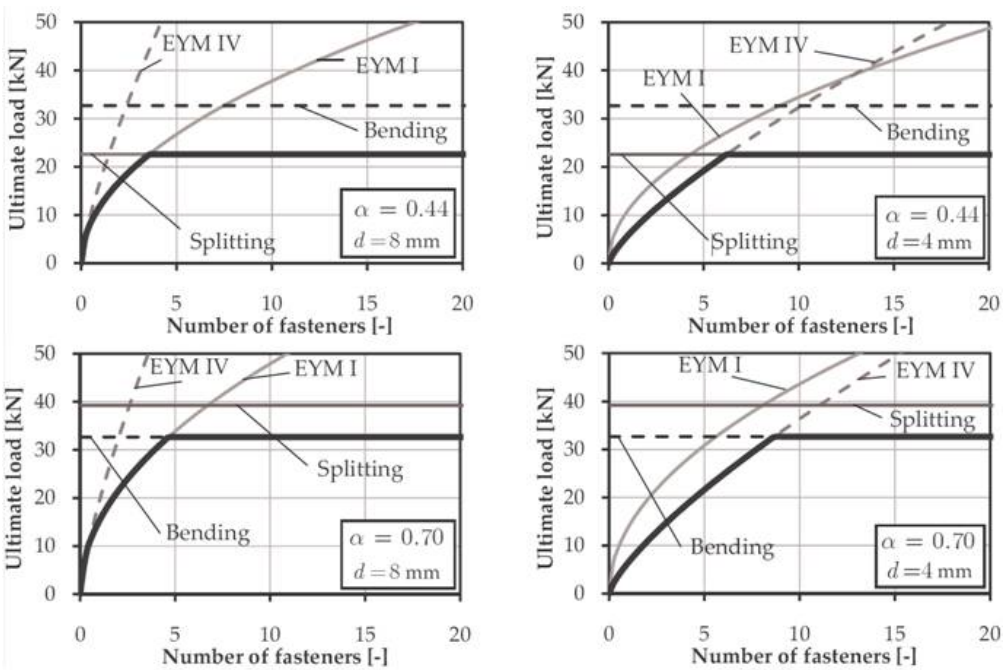

Figure 3. Ultimate load and associated failure mechanisms in four situations, as a function of the number of fasteners

Figure 4 shows some typical failure patterns observed from tests with rather slender nails ($t/d \approx 10$). All beam specimens were of equal geometry. The failure mode typically depends on the number of nails and hence. Few nails ($n = 5$) (Figure 4b and d) result in plastic hinges and substantial timber crushing. Increasing the number of nails results in splitting failure while the embedment zone remains undamaged (Figure 4a and c).

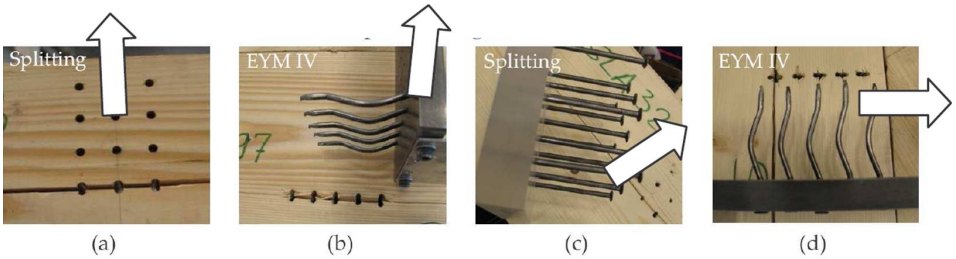

Figure 4. Typical failure patterns including the loading direction; (a) splitting, n = 12; (b) plastic hinges, n = 5; (c) splitting, n = 20; (d) plastic hinges, n = 5

What should be noticed from the charts presented is that splitting failure of a timber member is typically independent of the number of fasteners a connection is composed of. Also even rather slender fasteners ($t = 45$ mm, $d = 4$ mm) do not necessarily develop plastic hinges if the splitting strength is governing. This behaviour of dowel-type fastener connections is confirmed by experiments as discussed in Schoenmakers (2010) in detail.

Figure 5 shows typical load-slip measurements. The slip of the connection can be regarded as the plastic deformation (crushing) of the timber fibres in the embedment zone. In terms

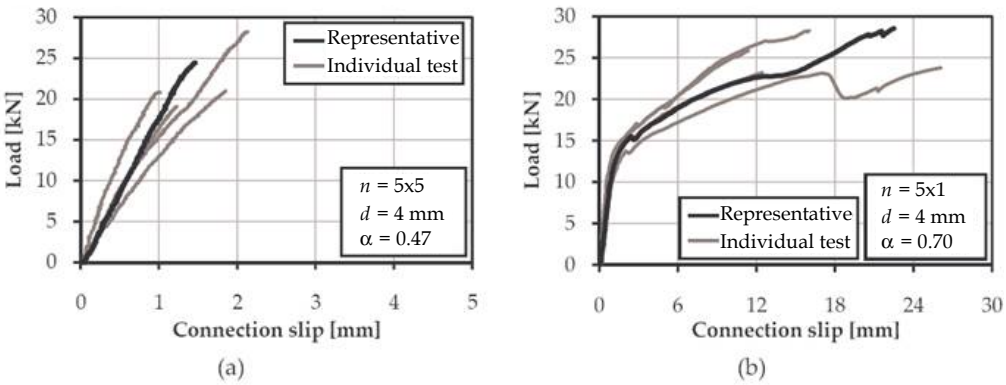

Figure 5. Typical experimental load-slip responses (a) linear-elastic response - splitting; (b) nonlinear elastic response - connection failure

of load-slip behaviour substantial differences among the failure mechanisms are observed as well. In case of splitting, the load-slip behaviour is linear-elastic up the failure, while in case of connection failure the response is elasto-plastic with significant hardening.

3 Analytical modelling of splitting strength

The splitting capacity is derived analytically utilising Linear Elastic Fracture Mechanics (LEFM). In this section, first the theory of the compliance method is outlined followed by an application of the theory to the situation of a single connection located at mid span of a simply supported beam. After that, the model is calibrated with experimental data resulting in an accurate prediction model of the load-bearing capacity. The model validity is shown by comparing (other) experimental data and the model predictions.

3.1 LEFM Compliance method

Crack propagation is analysed by considering the energy balance before and after a virtual crack extension. According to basic LEFM, a linear-elastic body of constant width t containing a crack of length λ, subjected to a (fixed) concentrated load F causing a displacement δ it follows for the energy released during an infinitesimal small crack extension:

$$\mathcal{G} = \frac{1}{t}\left(\frac{dE_{ext}}{d\lambda} - \frac{dE_{el}}{d\lambda}\right) = \frac{1}{t}\left(F\frac{d\delta}{d\lambda} - \frac{F}{2}\frac{d\delta}{d\lambda}\right) = \frac{F^2}{2t}\frac{dC}{d\lambda} \tag{1}$$

where C is the compliance (reciprocal stiffness) of the specimen. In LEFM the energy release rate $\mathcal{G}$ is defined as the decrease in potential energy of an element as a result of such a crack extension. The critical load for crack propagation (crack growth) now results from equation (2) (*e.g.* Gdoutos (2005)), by assuming an energy-based fracture criterion (i.e. $\mathcal{G} = \mathcal{G}_c$ - the energy release rate reaches its critical magnitude).

$$F_{crit} = \sqrt{\frac{2t\mathcal{G}_c}{\frac{dC}{d\lambda}}} \tag{2}$$

The critical energy release rate $\mathcal{G}_c$ basically is a material property and dependant on the fracture mode exposed to. Considering equation (2) reveals that the critical crack load F_{crit} can be predicted by deriving expressions of the compliance change due to infinitesimal crack extension $\frac{dC}{d\lambda}$.

3.2 *Analytical derivation*

Figure 6 shows the statics of half the beam structure (the total beam length is 2*l*). The model consists of an uncracked beam part (part 1) and a cracked beam part, the latter part modelled as two beam segments (part 2 and 3). All segments are modelled using Timoshenko-beam elements. At the crack tip, plane sections are assumed to remain plane according to Bernoulli's hypothesis. This is modelled by an element of infinite bending stiffness.

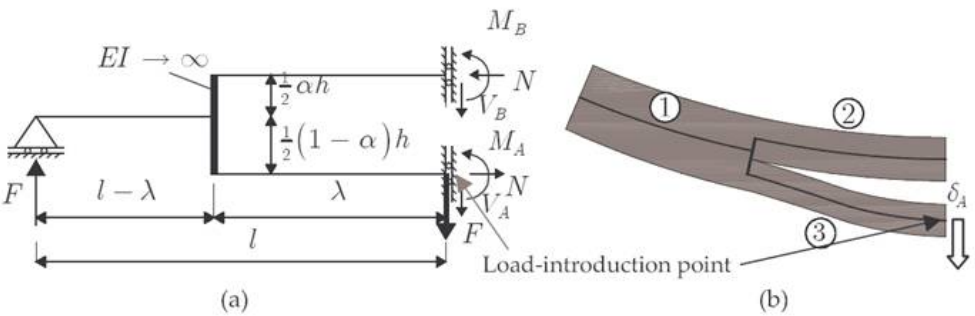

Figure 6. Modelling of structure; (a) statics of half the beam; (b) deformed shape and position of beam segments

By means of free-body diagrams, expressions for the internal forces and moments are derived for each beam segment, expressed in the crack length λ. The displacements and angular rotations are determined by an (strain) energy method and Castigliano's theorem (Timoshenko and Goodier (1951)). Having closed-form expressions of the internal forces and moments the compliance of the beam is expressed in terms of the crack length λ by equation (3).

$$\frac{\delta_A}{F} = C = \frac{6}{5Gth}\left(l - \lambda\left(1 - \frac{1}{\alpha}\right)\right) + \frac{1}{EI}\left(\frac{l^3}{3} - \frac{\lambda^3}{12}\left(1 - \frac{1}{\alpha^3}\right)\right) \tag{3}$$

where the moduli of elasticity and rigidity are expressed as $E = E_{11}$ and $G = G_{12}$, respectively (1st direction is parallel-to-grain, 2nd and 3rd directions both perpendicular-to-grain). Taking the derivative with respect to λ and substitution in equation (2) results equation (4) after multiplication with a factor 2 to account for symmetry. Equation (4) is the same as found by Jensen (2003) and by Van der Put (2005), by adopting the moment-area method.

$$F_{ult} = 2F_{crit} = 2t\sqrt{\frac{G\mathcal{G}_c h\alpha}{\frac{3}{5}(1-\alpha)+\frac{3}{2}\left(\frac{\lambda}{h\alpha}\right)^2\frac{G}{E}\left(1-\alpha^3\right)}} \tag{4}$$

Equation (3) shows that the compliance change $\frac{\partial C}{\partial \lambda}$ is independent of the beam span. Consequently, equation (4) holds for any connection located at mid span of a simply supported beam of arbitrary length, where the crack length λ is the only unknown variable. It should be recognized that in case of α = 0 the ultimate load F_{ult} = 0. In this case, the loaded edge distance h_e = 0 meaning basically that the connection does not exist, and hence, the ultimate load has no meaning.

The maximum critical load corresponds to a situation with λ → 0, i.e. only infinitesimal small cracks are present which have not yet propagated. In terms of FM, this implies the crack is always in an unstable equilibrium, i.e. $\frac{\partial(\mathcal{G}-\mathcal{G}_c)}{\partial\lambda} > 0$. Consequently, the energy released during crack propagation is higher than the critical energy release rate, and remains higher. Therefore, the ultimate load can be calculated by the reduced equation (5), resulting from equation (4) with λ → 0. For small crack lengths (λ → 0) Bernoulli's hypothesis does not hold. Assuming the Saint Venant length (at the load-introduction point) to be approximately equal to the depth of beam part 3 ($h\alpha$) shows that any discrepancy between model and reality will be of minor effect on the critical load.

$$F_{ult} = 2F_{crit} = 2t\sqrt{\frac{G\mathcal{G}_c h\alpha}{\frac{3}{5}(1-\alpha)}} \tag{5}$$

Figure 7 presents the critical load as function of the ratio half crack length/depth beam part 3. Since the equilibrium state is unstable in all conditions, the ultimate load is equal to

3.3 the critical load at crack initiation. Therefore, the crack extension rate is of minor interest. Model calibration

The parameter $\sqrt{G\mathcal{G}_c}$ typically represents the square root of the product of the modulus of rigidity and the critical energy release rate. Van der Put and Leijten (2000) suggest using the parameter $\sqrt{G\mathcal{G}_c}$ as a calibration parameter derived from experiments. This more robust approach is justified since the mode-mixture governing the mixed-mode fracture energy is generally unknown. Only the lower and upper bound can be given (both pure mode *I* and mode *II* fracture energies), hence $\mathcal{G}_{Ic} \le \mathcal{G}_c \le \mathcal{G}_{IIc}$, where $\mathcal{G}_{IIc} \approx 4\mathcal{G}_{Ic}$ according to tests performed by Stefansson (2001).

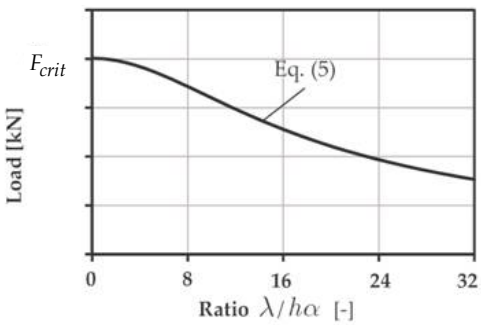

Figure 7. Ultimate load as function of the ratio half crack length and relative height

This calibration of the apparent fracture parameter $\sqrt{G\mathcal{G}_c}$ is performed extensively based on both experiments reported in literature and tests performed at TU/e. Over approximately 350 experiments were taken into consideration. The fracture parameter of all glulam specimens is statistically equal. Therefore, the average $\sqrt{G\mathcal{G}_c}$ = 14.9 N/mm$^{1.5}$ (cov = 22.3%) is taken as calibration parameter. For sawn specimens, it is shown that specimens tested at TU/e are different from specimens reported in literature. Therefore, the average $\sqrt{G\mathcal{G}_c}$ = 13.6 N/ mm$^{1.5}$ (cov = 16.7%) based on the Eindhoven results only is considered as calibration parameter. Accordingly, the ultimate load (splitting capacity) is predicted by equation (6):

$$F_{ult} = 2F_{crit} = 2t\sqrt{G\mathcal{G}_c}\sqrt{\frac{h\alpha}{\frac{3}{5}(1-\alpha)}}\ , \quad \sqrt{G\mathcal{G}_c} = \begin{cases} 14.9\ \text{N/mm}^{1.5} & \text{for gluelam} \\ 13.6\ \text{N/mm}^{1.5} & \text{for sawn} \end{cases} \tag{6}$$

The physical soundness of the results was verified by estimating the expected range of both G and $\mathcal{G}_c$ by means of statistics and statistical tests of significance (Schoenmakers (2010)).

Prior to calibration, it is verified that the experiments taken into consideration failed by splitting, by performing a detailed analyses of experiments in terms of governing failure mechanism using the models for both splitting capacity (as discussed in this article) and embedment strength (discussed in Schoenmakers (2010)). Model calibration studies (or explanation of test results) reported in literature mostly lack the distinction in failure modes observed (other failure mechanisms were included as well) and hence, these are of minor relevance (*e.g.* Ballerini (1999), Ballerini and Giovanella (2003), Ehlbeck *et al.* (1989)). In certain cases no attempts have been reported.

3.4 *Model validation*

The model validity was verified by comparing the predicted ultimate load and the experimentally observed ultimate load. In total, the model was compared with 899 experimental observations provided in literature, including a variety of multiple fastener connections (Figure 8). Experimental data considered are presented by Reshke *et al*. (2000), Lehoux and Quenneville (2004), Habkirk and Quenneville (2006), Ballerini (1999), Ballerini and Giovanella (2003), Möhler and Lautenschläger (1978), Möhler and Siebert (1980), Ehlbeck *et al*. (1989), and Yasumura *et al*. (1987). In general, good agreement between tests and predictions was observed.

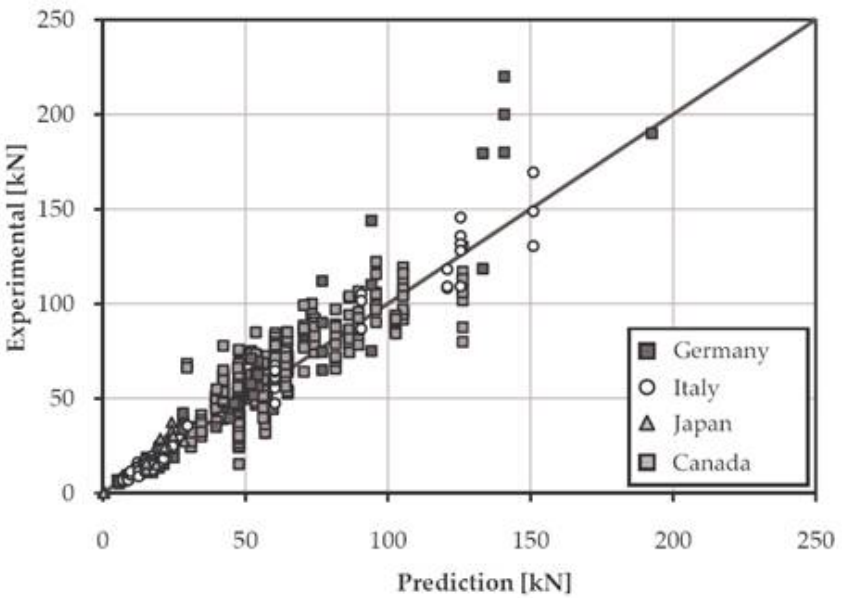

Figure 8. Model predictions versus experiments reported in literature

It should be recognized that the model calibration was based on a batch of approximately 350 specimens (including TU/e-tests), while the model validity shown in Figure 8 is based on approximately 900 specimens (only reported in literature). At the characteristic level (design rule), the model can be used with $\sqrt{G\mathcal{G}_c}$ = 10.8 N/mm$^{1.5}$ for glulam spruce and $\sqrt{G\mathcal{G}_c}$ = 9.9 N/mm$^{1.5}$ for sawn spruce (Schoenmakers (2010)).

4 Numerical modelling of splitting strength with a discrete crack

Generally, it is assumed the energy associated with fracture of connections perpendicular-to-grain is close to the mode *I* fracture energy G_{Ic} . This is verified using two numerical approaches; a discrete crack approach (this section) and a damage mechanics approach using cohesive elements (section 5). Inherent to both approaches is that the future crack path should be known. In this case this is not a limitation since cracking will always occur in line with the row of fasteners furthest from the loaded edge.

In this section the stress state of crack tips is evaluated by means of a discrete crack approach in the framework of FEM. The simulations use a 2D approach since 3D simulations as well as experiments show that the fasteners remain straight in case of splitting failure (Schoenmakers (2010)). By knowing the stress state, an estimate of the onset of cracking can be made using a fracture criterion. Basically, such an approach is in accordance with the classical fracture mechanics theory (Stress Intensity Factor (SIF) - approach, *e.g.* Gdoutos (2005)).

*4.1 **Parts, elements and mesh***

Two connections are modelled: a single fastener connection using d = 10 mm diameter holes, and a multiple fastener connection of n = 3 × 4 fasteners of d = 6 mm, spaced 4d. The beam cross-section is 45 × 220 mm² with a span of 1600 mm. Only the fastener holes are modelled, not the fasteners themselves. Three relative heights are considered, α = (0.3, 0.5, 0.7). All combinations of d and α have been modelled with the exception of d = 6 mm and α = 0.3, because in this instance the connection height is larger than the loaded edge distance which is physically impossible. The beam is meshed using fully-integrated hexahedral quadratic plane stress elements (CPS8 (ABQAUS v 6.7)).

The crack itself is modelled using an embedded line (seam) along which duplicate nodes are assigned. In a discrete crack model exhibiting sharp cracks, the strain field becomes singular at the crack tip. Including this singularity improves the accuracy of the contour integral evaluations, and consequently, of the stress and strain output. Therefore, the crack tip is meshed by a ring of 16 triangular collapsed quarter point quadratic elements (CPS6) (Figure 9). Accordingly, a $\frac{1}{\sqrt{r}}$ strain singularity is included by means of nodal translation (Figure 9b) with r the distance ahead of the crack tip. Local mesh refinement is adopted to

capture large stress concentrations to obtain accurate results for the SIFs, although not necessary for *J*-integral evaluation. Figure 10 presents the FE-model and the deformed shape, and a detail of the crack tip mesh.

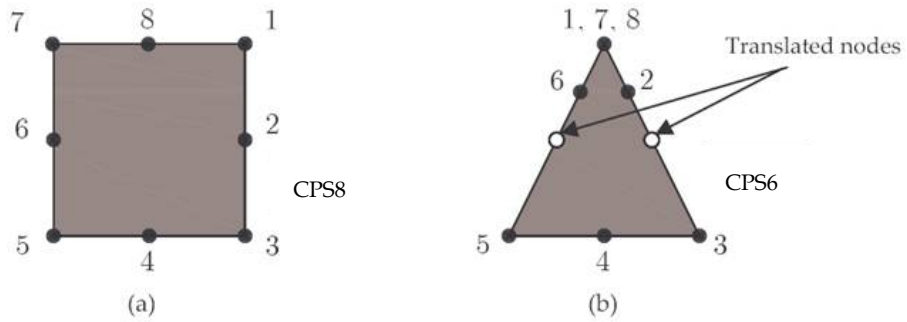

Figure 9. (a) (Regular) plane quadratic element; (b) Collapsed quarter point element

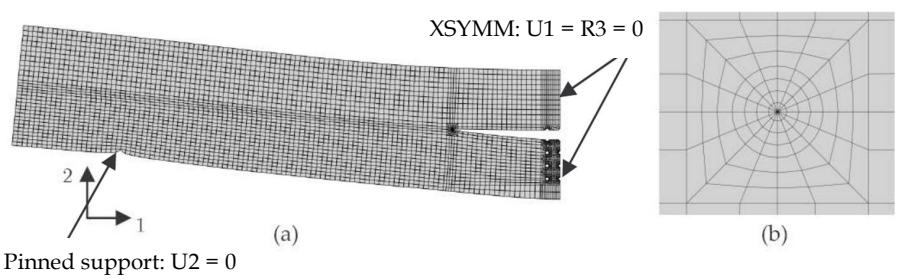

Figure 10. Discrete crack model; (a) deformed shape; (b) mesh detail of crack tip

4.2 ***Material properties***

The timber constitutive response is assumed linear-elastic in accordance with the basic assumptions of LEFM. This allows a contour integral evaluation in terms of energy release rate since in elastic cases it equals the evaluate *J*-integral ($\mathcal{G} = J$). Consequently, both can be estimated from the individual SIFs, (ABAQUS (2007)). The timber material is modelled using orthotropic elastic constants $E_{11} = 30$, $E_{22} = 16$, $G_{12} = 12000$ N/mm².

4.3 Boundary conditions, interactions and load

Due to symmetry, only half the specimen is modelled, and appropriate boundary conditions are specified at the symmetry plane (XSYMM, U1=R3=0). The pinned support prevents displacements in vertical direction. The load is introduced by a unit concentrated force at the pinned support. Kinematic coupling constraints are enforced preventing the holes from distorting (remain circular). In case of the multiple fastener connection, the displacements and rotations of all holes are coupled (and zero) using a multipoint constraint.

4.4 Solution procedure

ABAQUS/Standard is used as solver while the analyses are force controlled and geometrically linear (NLGEOMOFF). The stress state of the crack tip is evaluated using contour integrals. This requires defining the virtual crack extension direction, which is taken in line with the first principle beam axis, i.e. in line with the furthest row of fasteners from the loaded edge. According to ABAQUS (2007), multiple contours surrounding the crack tip are required to obtain an accurate solution, while the first and second contour should typically be ignored in elastic situations. Generally, the stress state of a crack tip is unique and highly dependent upon the crack length. Therefore, the crack length is extended manually and the stress state is computed for each pre-defined crack length. The size of the crack length increments varies among the simulations performed.

4.5 Validation of FE-model and results

Figure 11 presents the evolution of both mode *I* and mode *II* SIFs due to crack propagation associated with unit loading (F = 1 kN) (Unit SIF k_i , (i = *I*, *II*) - no capital K_i used to indicate this is the unit SIF). The numerical critical load is determined from the energy release rate (Figure 12b) by adopting the fracture criterion proposed by Wu (1967), i.e.:

$$\frac{K_I}{K_{Ic}} + \left(\frac{K_{II}}{K_{IIc}}\right)^2 \leq 1 \tag{7}$$

Since the analyses are linear, the load, the energy release rate and SIFs are proportional, and therefore, the critical load can be calculated by determining the load amplifier $^{\perp}$ to the unit load to satisfy the failure criterion ($F_{ult} = \Omega F_{unit}$). Figure 12a presents the numerical ultimate load and the analytical ultimate load given by equation (6).

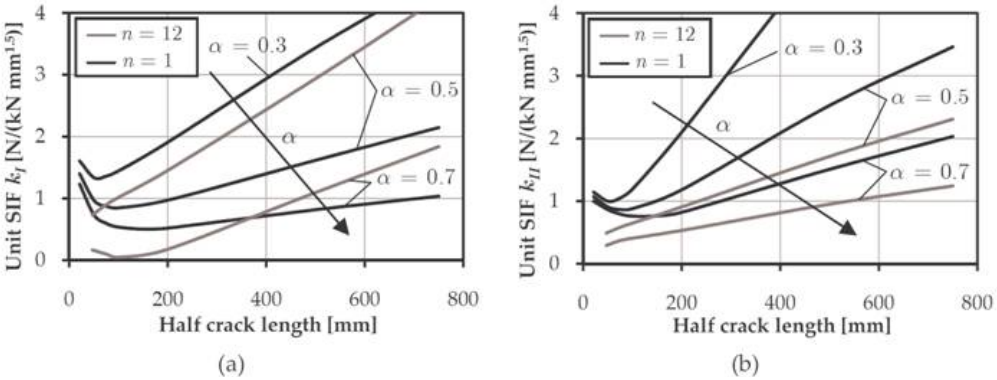

Figure 11. Unit stress intensity factors (Unit SIF); (a) mode I; (b) mode II

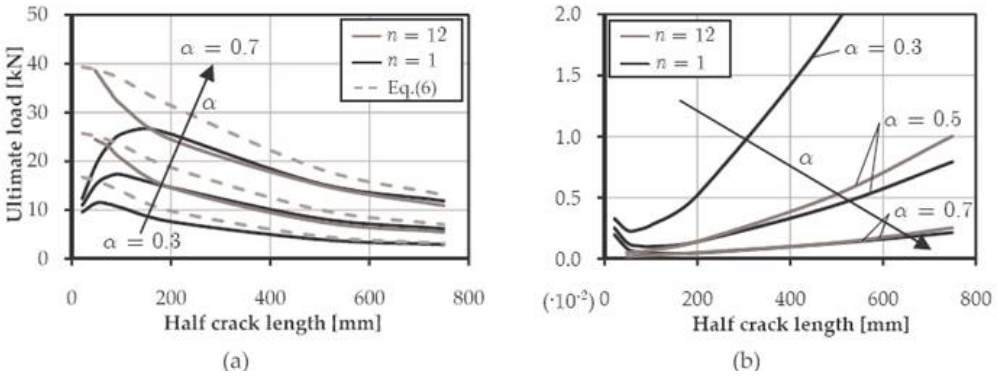

Figure 12. (a) numerical critical load determined with mixed-mode fracture criterion suggested by Wu (1967); (b) unit energy release rate

Figure 11 shows that the SIFs tend to decrease with increasing relative height α. Most SIFs tend to increase with increasing crack lengths after the crack length is sufficiently large ($\lambda \geq 75$ mm), indicated by the minimum (*e.g.* Figure 11 a). Estimating the ultimate load from the energy release rates suggests that in case of single fastener connections, the crack length may increase without resulting unstable crack propagation (indicated by a maximum in (Figure 12a)). Consequently, the critical crack length is approximately $\lambda_{crit} \approx$ 75 mm. Hence, the crack is in a stable equilibrium situation for smaller crack lengths. This is a result of the crack tip being still in Saint Venant's length of the load-introduction. The cracks in the multiple fastener connection are always unstable. Both numerical and analytical ultimate loads agree well. Also the post-fracture behaviour governed by the size

of the cracks shows reasonable agreement, although the model presented suggests less decrease of ultimate load with increasing crack length.

5 Numerical modelling of splitting strength with a progressive damage approach

In this section progressive fracture is modelled by a damage mechanics approach using cohesive elements. It is chosen to model a n = 3 × 4 connection with d = 6 mm diameter fasteners, and a n = 5 × 5 connection with d = 4 mm fasteners since these connections have shown to fail in pure splitting. The beam cross-section is 45 × 220 mm² and the span is 1600 mm.

5.1 Parts, elements and mesh

The FE-model consists of four 3D solid deformable parts. The timber beam is separated in a top and bottom part. In-between, a fracture layer is modelled along the full ligament length. The bottom beam part and the bottom side of the fracture layer are kinematically coupled using a tie-constraint. The same is done for the top layer side. This method allows both independent meshing and mesh densities of both beam parts. These tie-constraints behave like a master-slave contact pair in which the fracture layer acts as the slave. Due to symmetry, only one quarter of the specimen is modelled. Figure 13 gives an overview of the FE-model (for clarify, the symmetry planes are left out).

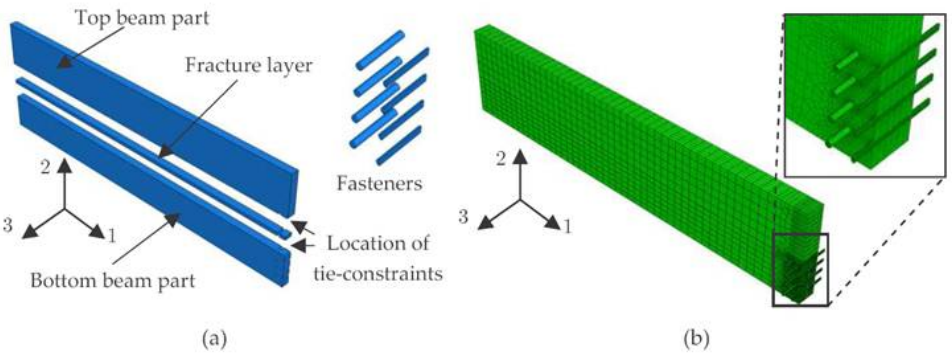

Figure 13. FE-model using a cohesive fracture layer; (a) all individual parts extracted; (b) meshed half FE-model and detail of connection zone

The timber and steel are meshed using hexahedral linear continuum elements using reduced integration schemes and enhanced hourglass control (C3D8R). The fracture layer is meshed using linear cohesive elements (COH3D8). After meshing, the coordinates of all nodes of the fracture layer are adjusted exactly along the ligament, resulting the geometrical thickness of the cohesive layer is reduced to zero (the top and bottom surface are geometrically equal) (Figure 14). Mesh convergence studies show that only three elements over the beam thickness are sufficient to obtain mesh convergence (since the fasteners remain straight).

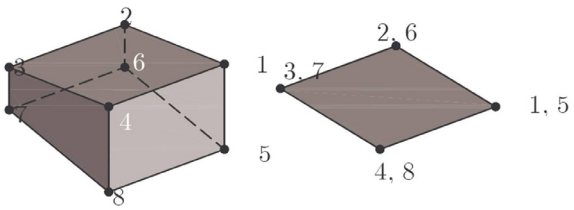

Figure 14. Adjusted nodes providing a geometrical zero thickness of single cohesive element

5.2 ***Material properties***

Preliminary simulations show that the timber mainly remains in the elastic stage during the entire analyses. The steel fasteners remain straight during the analyses and hence, elastic constitutive responses are implemented. For the fracture layer a traction-separation model is adopted to accurately model the fracture performance of timber where linear-elastic behaviour up to attaining the ultimate load is assumed.

Up to damage initiation, the response is linear-elastic governed by an elastic constitutive matrix $[K_o]$ relating the nominal tractions (stresses) to the nominal strains across the interface.

Mixed-mode fracture tests are reported by Stefansson (2001). In these tests, the notched timber specimen was loaded at different ratios of both normal and shear stress. During crack propagation, the crack lengths and opening displacements were recorded.

Based on these test tests, the components of $[K_o]$ are considered uncoupled,

with K_n = 150 N/mm² and $K_s = K_t$ = 100 N/mm², where indices (n, s, t) represent

the normal, the first and the second shear direction, respectively. Damage initiation is defined in terms of a quadratic interaction equation combining both normal and shear tractions (equation (8)).

$$\left(\frac{\langle t_n \rangle}{t_n^0}\right)^2 + \left(\frac{t_s}{t_s^0}\right)^2 + \left(\frac{t_t}{t_t^0}\right)^2 = 1 \tag{8}$$

In this equation t_i , (i = s, n, t)are the traction components in either normal or one of both shear modes, and t_i^0 , (i = s, n, t)their corresponding critical values, i.e. the tensile strength perpendicular-to-grain $t_i^0 = f_{t;90}$ =3.0 N/mm² and shear strength $t_s^0 = t_t^0 = f_{v;12}$ = 10.0 N/mm² , respectively. The angular brackets indicate that an average value over the elements volume is computed. Figure 15 presents the quadratic interaction equation (8) and the mixed-mode test data reported by Stefansson (2001). For comparison, the maximum stress criterion and the mixed-mode interaction equation suggested by Wu (1967) are included. Comparison of the mixed-mode data and the quadratic criterion implemented (Figure 15) suggests that the numerical solution will overestimate the experimental ultimate load, in general. Since fracture in the cases studied is close to mode I fracture (normal stresses governing), no attempts have been made to implement a user-defined damage criterion (damage models presented are available in ABAQUS) as results were sufficiently satisfying (despite Figure 15 suggesting a linear relation).

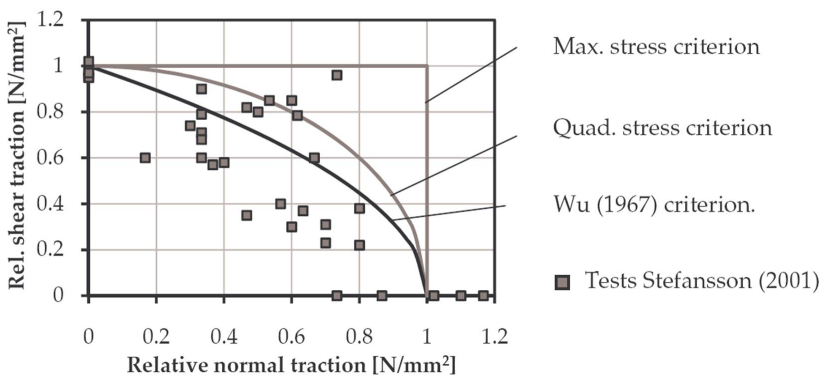

Figure 15. Damage initiation criteria

The damage evolution (softening) law describes the rate at which the material stiffness is degraded once the corresponding initiation criterion is satisfied. An energy-type law with

the fracture energy as the area enclosed by the softening curve is implemented. In this respect, the mixed-mode fracture criterion according to Petersson (2002) is adopted where the critical strain energy release rates are taken as $\mathcal{G}_{Ic} = \frac{1}{4}\mathcal{G}_{IIc} = 300$ J/m².

The overall damage in the material is represented by a scalar damage variable D. Initially, $D = 0$ (undamaged) and it evolves monotonically towards $D = 1.0$ (fully damaged). It therefore defines the post-damage initiation behaviour since it affects the individual traction and stiffness components. Consequently, progressive damage is characterized by progressive degradation of the material stiffness, driven by the damage process. Accordingly, the traction components are defined by equation (9) (reference can be made to Figure 16 for parameters):

$$t_i = \begin{Bmatrix} K_i\delta_i & \delta_i^{\max} \le \delta_i^0 \\ (1-D)K_i\delta_i & \delta_i^0 < \delta_i^{\max} < \delta_i^f \\ 0 & \delta_i^{\max} \ge \delta_i^f \end{Bmatrix} i = (n,s,t) \tag{9}$$

Despite that timber exhibits approximately exponential softening behaviour it is chosen to use an energy-equivalent linear softening model to improve convergence. This can be noticed from Figure 16; if exponential softening is used, the critical crack opening in certain cases may become excessive as a result of a both fixed critical stress and energy, while the damage variable is mixed-mode dependent. It is recognized that adopting linear instead of exponential softening affects the degradation rate.

For numerical convenience in mixed-mode conditions, the individual displacement components are combined by an effective displacement according to equation (10):

$$\delta_m = \sqrt{\langle \delta_n \rangle^2 + \delta_s^2 + \delta_t^2} \tag{10}$$

The damage variable is defined by equation (11):

$$D = \frac{\delta_m^f(\delta_m^{\max} - \delta_m^0)}{\delta_m^{\max}(\delta_m^f - \delta_m^0)} \tag{11}$$

where $\delta_m^{\max}$ is the maximum displacement attained during the analysis, δ_m^f the effective displacement at complete separation, and δ_m^0 the effective displacement at damage

initiation (see also Figure 16 , where t_m^0 the effective maximum traction). Definition of the constitutive thickness of the fracture layer ensures that the nominal strain is equal to the separation (ABAQUS (2007)).

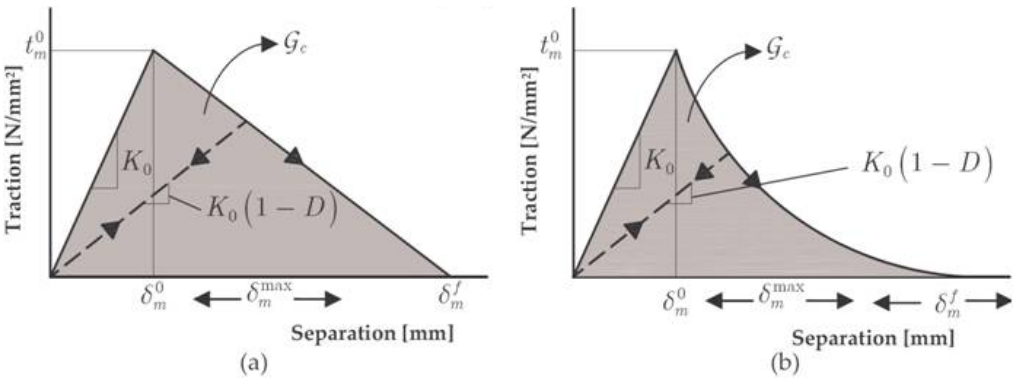

Figure 16. Constitutive response of cohesive elements; (a) linear softening; (b) exponential softening

*5.3 **Boundary conditions, interactions and load***

Appropriate boundary conditions are specified at both symmetry planes (1st symmetry plane i.e. XSYMM (U1=U2=R3=0), 2nd symmetry plane YSYMM (U1=U3=R2=0)). A master-slave constraint equation at the location of the pinned support ensures displacements in both the first and second direction, and rotations along the third axis are governed by the master mode, simulating a line support. Load is applied by a prescribed displacement in de second direction at the pinned support. To model the stiff steel side members, the displacements and rotations of all fastener edges are coupled using a multipoint constraint (fully clamped). The model is supported at the top-side over-length of the fasteners over a length of 15 mm. As a result of the dowel over-length, a horizontal gap of 2 mm in the third direction between the load and the timber block is left clear, in accordance with the experimental set-up. The interactions between fasteners and timber are modelled using contact elements.

*5.4 **Solution procedure***

Since the definition of the cohesive elements is based on a progressive degraded stiffness method, severe convergence problems will often occur using implicit solvers such as ABAQUS/Standard. ABAQUS (2007) suggests using viscous regularization of the constitutive equations, resulting the tangent stiffness matrix of the softening material to be

positive for sufficiently small time increments. The traction-separation law can be regularized using viscosity permitting stresses to be outside the limits set by the tractionseparation law. The regularization process involves using a viscous stiffness degradation variable D_v , defined by the evolution equation $\frac{\partial}{\partial t} D_v = \frac{1}{\mu_v}(D - D_v)$. The viscosity parameter μ_v represents the relaxation time of the viscous system and D is the degradation variable evaluated in the inviscid backbone model (ABAQUS (2007)). This procedure is schematically represented by Figure 17. The viscosity parameter μ_v should be taken typically small in order to approximate the actual behaviour sufficiently accurate; small compared to the characteristic time increment. Viscous regularization usually helps improve the rate of convergence of the model in the softening regime, without compromising results.

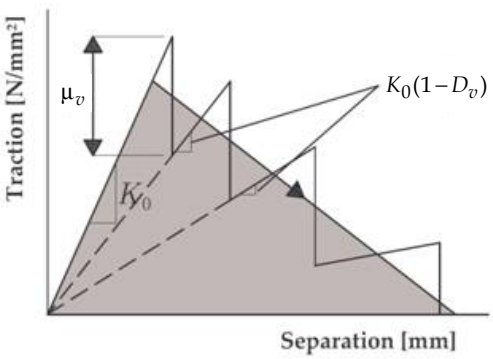

Figure 17. Schematic representation of viscous regularization

Adopting this concept requires that the approximate amount of energy associated with viscous regularization remains small compared to the total internal energy of the system (calculated by ABAQUS), typically in the order of 1%. If the viscous energy becomes larger, the entire simulation is likely to run on viscosity and does not represent the actual structural behaviour any more. The cohesive elements are removed from the analyses when degraded completely. During the analyses, the amount of viscous energy dissipation was monitored carefully (Schoenmakers (2010)). Mostly, the viscosity parameter μ_v = 0.001 is taken although sometimes it is decreased even more.

5.5 *Validation of FE-model and results*

Validation of the FE-model is performed in terms of load-slip response and ultimate load. Figure 18 shows the damage evolution of the fracture layer at the onset of cracking (damage initiation, Figure 18a), and during crack propagation (Figure 18b). Non-damaged elements still behave elastically, and failing elements are in the softening regime of the constitutive response (Figure 18a).

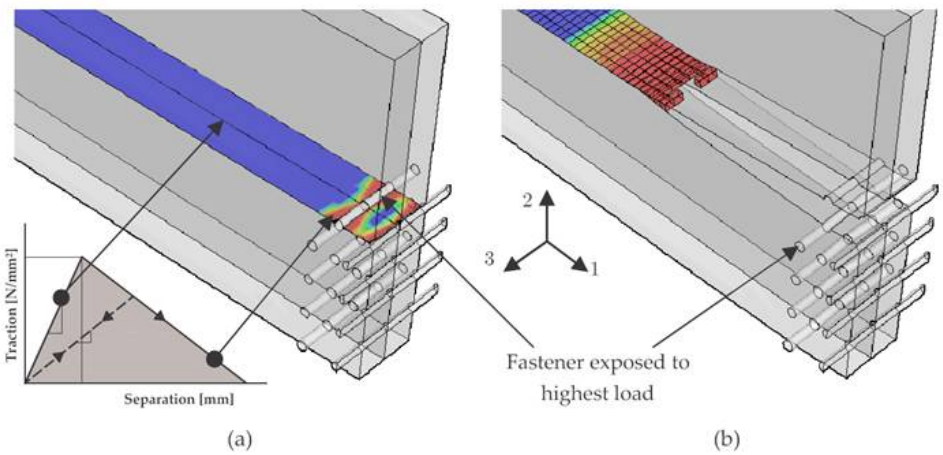

Figure 18. Damage evolution; (a) onset of cracking; (b) crack propagation (colour figure at www.heronjournal.nl)

The numerical load-slip response is nearly linear-elastic up to failure where a slight bent-off is observed prior to attaining the ultimate load. The numerical model tends to be too stiff (approximately 20%) compared to the experimental load-slip curve. Table 1 presents the numerical ultimate load obtained for several relative heights. The parameter $\sqrt{G\mathcal{G}_c}$ is calculated and listed. Both simulations with the connection at $\alpha = 0.44$ and $\alpha = 0.47$ correspond to the experimental investigations described in (Schoenmakers (2010)) with F_{ult} = 19.3 kN ($\sqrt{G\mathcal{G}_c}$ = 12.7 N/mm$^{1.5}$) and F_{ult} = 22.8 kN ($\sqrt{G\mathcal{G}_c}$ = 14.0 N/mm$^{1.5}$), respectively.

No substantial differences in ultimate load of both connections are observed. Additionally, it is concluded that the parameter $\sqrt{G\mathcal{G}_c}$ remains approximately constant, for all α except $\alpha = 0.8$. In general good agreement between experiments and numerical simulations is

achieved, except for $\alpha = 0.8$ for which the numerical ultimate load substantially over-estimates the expected load (equation (5)). In this case (large loaded edge distance relative to the total beam depth) the connection is situated far into the bending-compressive zone what may result in reinforcing effects preventing crack propagation, and resulting crack closure. Details are included in Schoenmakers (2010).

6 Summary and conclusions

Both numerical and analytical techniques have been adopted to model fracture in case of a single connection located at mid span of a simply supported beam. Numerical analyses have been performed using a progressive damage approach (cohesive elements) and a discrete crack approach. The results of the numerical simulations and analytical model are in good agreement with the results of an experimental program.

A finite element (FE) discrete crack approach appears to be an appropriate tool for studying the stress state around the crack at crack propagation, form which the ultimate load can be predicted. An FE damage mechanical approach (in 3D) shows that basic assumptions made in 2D (plane section) are appropriate in terms of fastener deformation and energy released during crack extension.

The splitting capacity is independent on the fastener configuration, the fastener type (nails or dowels) and diameter enabling a simplified analytical approach. The analytical models are based on the compliance method (LEFM), accounting for the timber thickness and connection location with respect to the beam depth. A calibration procedure is performed with regard to the apparent fracture parameter $\sqrt{G\mathcal{G}_c}$, using an extensive experimental data base taken from literature and extended with experiments performed at Eindhoven

Table 1: Numerical results obtained from cohesive element approach

	α	0.44	0.47	0.50	0.60	0.70	0.80
$n = 3 \times 4$	F_{ult} [kN]	21.1	N/A	21.8	25.8	34.7	89.1
	$\sqrt{G\mathcal{G}_c}$ [N/mm$^{1.5}$]	13.9	N/A	12.7	12.2	13.2	25.8
$n = 5 \times 5$	F_{ult} [kN]	N/A	21.5	22.8	26.3	33.9	84.2
	$\sqrt{G\mathcal{G}_c}$ [N/mm$^{1.5}$]	N/A	13.2	13.2	12.5	12.9	24.4

University of Technology. Prior to calibration, it is verified that the experiments taken into consideration failed by splitting. The splitting capacity in terms of $\sqrt{G_c}$ of glulam timber beams is significantly higher than that of sawn timber beams. The critical energy release rate associated with fracture induced by dowel-type fastener connections is close to mode *I* values, as shown by numerical simulations.

The analytical model presented may be included in upcoming design standards due its ability to accurately predict the splitting capacity perpendicular-to-grain of timber beams when loaded by mechanical connections.

Acknowledgement

The author wishes to acknowledge the financial support provided by the Dutch Technology Foundation STW, applied science division of NWO and the technology Program of the Ministry of Economic Affairs to conduct this research.

References

All figures in this paper are taken from the dissertation of Schoenmakers (2010), entitled *Fracture and failure mechanisms of timber loaded perpendicular to the grain by mechanical connections*. Eindhoven University of Technology, Eindhoven, the Netherlands. ISBN: 978- 90-386-2223-1.

[1] ABAQUS (2007): ABAQUS v6.7 Documentation. Hibbitt, Karlsson and Sorensen, Simulia, ABAQUS, Inc., Dassault Systèmes, USA.

[2] Ballerini, M. (1999): A new set of experimental tests on beams loaded perpendicular-to-grain by dowel-type joints. *Proceedings of CIB-W18* / paper 32-7-2, Graz, Austria.

[3] Ballerini, M. and Giovanella, A. (2003): Beams transversally loaded by dowel-type joints: influence on splitting strength of beam thickness and dowel size. *Proceedings of CIB-W18* / paper 36-7-7, Colorado, USA.

[4] Ehlbeck, J. and Görlacher, R. (1983): *Tragverhalten von Queranschlüssen mittels Stahlblechformteilen, insbesondere Balkenschuhe, im Holzbau*. Forschungsbericht der Versuchsanstalt für Stahl, Holz und Steine, Abt. Ingenieurholzbau, Universität Fridericiana, Karlsruhe, Germany.

[5] Ehlbeck, J. and Görlacher, R. (1995): Tension perpendicular to the grain in joints. Structural Timber Education Program (STEP), volume 1, lecture C2, *Bemessung und Baustoffe*, Düsseldorf, Germany.

[6] Ehlbeck, J., Görlacher, R., and Werner, H. (1989): Determination of perpendicular-to-grain tensile stresses in joints with dowel-type fasteners, a draft proposal for design rules. *Proceedings of CIB-W18A* / paper 22-7-2, Berlin, Germany.

[7] Gdoutos, E.E. (2005): *Fracture Mechanics - an introduction*. 2nd edition, Springer, Dordrecht, The Netherlands. ISBN: 1-4020-2863-6.

[8] Habkirk, R. and Quenneville, J.H.P. (2006): Bolted wood connections loaded perpendicular-to-grain: effect of wood species. *Proceedings of WCTE 2006*, Portland (OR), USA.

[9] Jensen, J.L. (2003): Splitting strength of beams loaded by connections. *Proceedings of CIB-W18*/ paper 36-7-8, Colorado, USA.

[10] Jensen, J.L., Gustafsson, P.J., and Larsen, H.J. (2003): A tensile fracture model for joints with rods or dowels loaded perpendicular-to-grain. *Proceedings of CIB-W18* / paper 36-7- 9, Colorado, USA.

[11] Johansen, K.W. (1949): Theory of timber connections. International Association of Bridge and Structural Engineering (IABSE), Publication 9, Basel, Switzerland.

[12] Lehoux, M.C.G. and Quenneville, J.H.P. (2004): Bolted wood connections loaded perpendicular-to-grain, a proposed design approach. *Proceedings of CIB-W18* / paper 37-7-4, Edinburgh, Scotland.

[13] Meyer, A. (1957): Die Tragfähigkeit von Nagelverbindungen bei statischer Belastung. *Holz als Roh- und Werkstoff* 15: 96-109.

[14] Möhler, K. and Lautenschläger, R. (1978): *Grobflächige Queranschlüsse bei Brettschichtholzträger*. Forschungsbericht des Lehrstuhls für Ingenieurholzbau und Baukonstruktionen, Universität Fridericiana, Karlsruhe, Germany.

[15] Möhler, K. and Siebert, W. (1980): *Ausbildung von Queranschlüssen bei angehängten Lasten an Brettschichtholzträger*. Forschungsbericht des Lehrstuhls für Ingenieurholzbau und Baukonstruktionen, Universität Fridericiana, Karlsruhe, Germany.

[16] Petersson, H. (2002): Energy release rate analysis. Fracture mechanics models for strength analysis of timber beams with a hole or a notch - a report of *RILEM TC-133*, Lund, Sweden.

[17] Reshke, R.G., Mohammad, M., and Quenneville, J.H.P. (2000): Influence of joint configuration parameters on strength of perpendicular-to-grain bolted timber connections. *Proceedings of WCTE 2000*, Whistler, British Columbia, Canada.

[18] Schoenmakers, J.C.M. (2010): *Fracture and failure mechanisms in timber loaded perpendicular to the grain by mechanical connections*. Dissertation, Eindhoven University of Technology, Eindhoven, the Netherlands. ISBN: 978-90-386-2223-1.

[19] Stefansson, F. (2001): *Fracture analysis of orthotropic beams - Linear elastic and non- linear methods*. Licentiate dissertation, Lund University, LTH, Structural Mechanics, Lund, Sweden. ISSN: 0281-6679.

[20] Timoshenko, S.P. and Goodier, J.N. (1951): *Theory of elasticity*. 2nd edition, McGraw-Hill Book Company, Inc., New York, USA.

[21] Van der Put, T.A.C.M. (1992): Energy approach for fracture of joints loaded perpendicular to the grain. *Proceedings of COST 508*: Wood Mechanics. Edited by Morlier, P., Valentin, G. and Seoane, I., Bordeaux, France.

[22] Van der Put, T.A.C.M. (2008): Derivation of the bearing strength perpendicular to the grain of locally loaded timber blocks. *Holz als Roh- und Werkstoff* 66: 409-417.

[23] Van der Put, T.A.C.M. (2005): *A new consistent theory of fracture mechanics of wood*. Publication of Delft Wood Science Foundation, Delft, The Netherlands.

[24] Van der Put, T.A.C.M. and Leijten, A.J.M. (2000): Evaluation of perpendicular to grain failure of beams caused by concentrated loads of joints. *Proceedings of CIB-W18* / paper 33-7-7, Delft, The Netherlands.

[25] Wu, E.M. (1967): Application of Fracture Mechanics to Anisotropic Plates. *Journal of Applied Mechanics* 34 (4): 967-974.

[26] Yasumura, M., Murota, T., and Sakai, H. (1987): Ultimate properties of bolted joints in glued-laminated timber. *Proceedings of CIB-W18* / paper 20-7-3, Dublin, Ireland.